Cement and Concrete Research 53 (2013) 196–210

Contents lists available at ScienceDirect

Cement and Concrete Research

journal homepage: http://ees.elsevier.com/CEMCON/default.asp

A coupled mechanical and chemical damage model for concrete affected by alkali–silica reaction ☆

Rossella Pignatelli [a,b,*], Claudia Comi [a], Paulo J.M. Monteiro [c]

[a] Department of Civil and Environmental Engineering, Politecnico di Milano, Piazza L. da Vinci 32, 20133 Milano, Italy
[b] Lombardi Ingegneria S.r.l., Via Giotto 36, 20145 Milano, Italy
[c] Department of Civil and Environmental Engineering, University of California, Berkeley, CA 94720, USA

ARTICLE INFO

Article history:
Received 18 January 2013
Accepted 18 June 2013

Keywords:
Alkali-Aggregate Reaction (C)
Degradation (C)
Concrete (E)
Damage theory
Double-layer theory

ABSTRACT

To model the complex degradation phenomena occurring in concrete affected by alkali–silica reaction (ASR), we formulate a poro-mechanical model with two isotropic internal variables: the chemical and the mechanical damage. The chemical damage, related to the evolution of the reaction, is caused by the pressure generated by the expanding ASR gel on the solid concrete skeleton. The mechanical damage describes the strength and stiffness degradation induced by the external loads. As suggested by experimental results, degradation due to ASR is considered to be localized around reactive sites. The effect of the degree of saturation and of the temperature on the reaction development is also modeled. The chemical damage evolution is calibrated using the value of the gel pressure estimated by applying the electrical diffuse double-layer theory to experimental values of the surface charge density in ASR gel specimens reported in the literature. The chemo-damage model is first validated by simulating expansion tests on reactive specimens and beams; the coupled chemo-mechanical damage model is then employed to simulate compression and flexure tests results also taken from the literature.

1. Introduction

The long term behavior of concrete structures may depend on various chemo-physical damage phenomena. Among them the degradation induced by the alkali–silica reaction (ASR) is of particular concern for the safety assessment of several concrete dams and bridges built decades ago. This reaction, occurring between the amorphous or poorly crystallized silica contained in some types of aggregates and the alkali from the cement paste, produces a gel that, in the presence of water, exerts a pressure on the solid skeleton causing overall swelling and microcracks formation in concrete.

Modeling is needed to compute the current safety level of a structure affected by ASR and to plan the required retrofit provisions. Various approaches to the problem have been proposed in the literature, which differ on the scale at which the phenomenon is observed: microscopic, mesoscopic and macroscopic models have been developed and a comprehensive list of the different models can be found e.g. in [1]. Within the macroscopic chemo-mechanical approach, various poro-mechanical models (e.g. [2–5]), consisting of a concrete skeleton and an expansive gel acting in parallel, have been proposed and successfully applied to describe the structural effects due to ASR. However, these works have been focusing on the correct prediction of the overall response of the experimentally measured expansion and, in some cases, in terms of macro-cracks formation but no attempt was made to compare the predicted values of the gel pressure with the experimental ones.

It has been difficult to obtain the values of the gel pressure by direct mechanical tests. Some of the few experimental data can be found in [6] and [7]. An alternative experimental strategy was proposed in [8] and then in [9], where the electrical double-layer theory was used to interpret the swelling mechanism of the alkali–silica gel and the gel pressure was estimated using the experimental values of the surface charge density measured on silica gel specimens.

In the same line of research, starting from the experimental data published in [10] on the surface charge density measured on alkali–silica gel specimens collected in Furnas dam (Brazil), the present work applies the electrical diffuse double-layer theory to estimate the gel pressure exerted on the concrete matrix. The obtained values are in agreement with the values measured with mechanical tests.

On the contrary, when using existing poromechanical models (as e.g. in [2–5] and [11]) the prediction of the gel pressure turns out to be one order of magnitude higher than the experimental one, as also remarked in [12]. When formulating a model at the mesoscale, as in poromechanical standard models, the different phases are homogenized and considered to entirely act in parallel and, hence, the deterioration of the concrete skeleton is smeared homogeneously. As discussed in [13] and [14], at the micro-scale the reaction gel is very localized, either at the interface between aggregates and cement paste or within the

☆ Part of this work was conducted while R. Pignatelli was visiting scholar at UC Berkeley.

* Corresponding author at: Department of Civil and Environmental Engineering, Politecnico di Milano, Piazza L. da Vinci 32, 20133 Milano, Italy. Tel.: +39 02 2399 4215; fax: +39 02 2399 4220.
E-mail addresses: rossellapignatelli@gmail.com (R. Pignatelli), comi@stru.polimi.it (C. Comi), monteiro@ce.berkeley.edu (P.J.M. Monteiro).

0008-8846/$ – see front matter © 2013 Elsevier Ltd. All rights reserved.
http://dx.doi.org/10.1016/j.cemconres.2013.06.011

aggregate, depending on the type and size of the aggregates. Microscopic observations (see e.g. [7])) show a severe damage only in the neighborhood of the reactive sites and large portions of concrete remain undamaged. At the micro-scale, in [12] the cause of cracking of slow reacting aggregates was related to the gel pressure by a fracture energy approach. This approach, as detailed in [14], can also be used to interpret the effects of the size of the aggregates on the ASR damage evolution. In the present work, at difference from the above cited contributions, we focus on the mesoscale and we develop a new model for concrete affected by the ASR, still through the phenomenological approach of poromechanics. In this line, we consider a single solid phase, the homogenized concrete skeleton, including cement paste, aggregates and non-connected porosity. The model, aimed to structural modeling, captures the reaction at a macro-scale and, to obtain more realistic results of the gel pressure and overall damage values, it suggests a connection between the macroscopic approach and some experimental information at the micro-scale. Analogously to [2,4,11], here a two-phase poromechanical model is obtained, but now two porosities are introduced: the common concrete porosity filled by the gel and an additional porosity due to the ASR chemical damage. The chemical degradation of concrete is described by the microscopic chemical damage d, an isotropic internal variable depending only on the reaction advancement. In the proposed mesoscale poromechanical model, an additional variable ω represents, in phenomenological manner, the portion of the concrete skeleton acting in series with the gel and therefore the portion which is not damaged by the gel pressure. The maximum values of the chemical damage d and the variable ω are determined by using the value of gel pressure obtained from the diffuse double-layer theory, and the experimental values of the reduction in Young's modulus of reacted specimens.

The effect of varying moisture conditions is also included in the model through the dependence on the degree of saturation. The degradation induced by the external loads is described by another independent damage internal variable, the mechanical damage, which depends on the overall stress and affects both the concrete skeleton and the gel. The model is validated by simulating the experimental tests on reacted concrete cylindrical specimens axially loaded and confined with steel rings reported in Multon [15] and the compression tests and the three point bending tests reported in Giaccio et al. [16]. Finally the model is used to simulate the structural tests performed by Multon and Toutlemonde [17] on plain reactive concrete beams subject to varying moisture conditions at constant temperature.

2. Computation of the ASR gel pressure

2.1. Double layer theory

In the alkali–silica reaction, the highly-charged surfaces of amorphous silica contained in some types of aggregates used in concrete mixtures interact with the alkaline pore solution of concrete and the reaction leads to the formation of a gel that can be expansive in the presence of water.

The amorphous silica are very reactive with aqueous solutions because the silicon tetrahedra are organized in a random three-dimensional structure without a regular arrangement, with defects, holes and large specific surface area which facilitate the interaction with the pore solution. In the presence of moisture the silica structure is depolymerized by hydration and the unbalanced charges at the surface of the dissolved silica particles are neutralized, hydroxyl groups OH^- linking to the positively-charged silicon ions and hydrogen cations H^+ to the negatively-charged oxygen ions, as shown in Fig. 1a and b. Since the interatomic bond Si – O – Si is stronger than the hydrogen bond O – H at the particle surfaces, silica surface is left with a weakly acidic character. When the silica particles are immersed in strongly alkaline solution, as in the case of concrete, where Na^+ and K^+ are present, the hydrogen cations H^+ at the silica surface are replaced by the alkaline cations Na^+, which create a characteristic double layer of counterions around the silica particles, as described in [18]. Fig. 1c and d shows the double-layer formed by the negative charges on particle surface and the attracted positive ions, the anions being repealed.

When two materials are in contact, the surface effects have a very important role in the prediction of the overall behavior. Since we have a colloidal system (sol) composed of dissolved silicate particles surrounded by a diffuse layer of cations and ions dispersed in the pore solution, it is expected that the gel expansion is determined by interface phenomena. The importance of surface chemistry has been long recognized in soil mechanics to interpret the flocculation and swelling of clays and other porous materials in contact with electrolyte solutions (see e.g. [6,19,20] and [21]). Prezzi et al. [8] investigated the importance of surface colloid chemistry in concrete deterioration and obtained a quantitative estimate of the expansive pressure in concrete induced by alkali–silica reaction by applying the Gouy–Chapman model of the diffuse part of the electric double layer ([22]) to the experimental results reported in [23]. According to the model proposed in [8], when concrete is exposed to air or during a drying event, the distance between colloidal particles decreases until the attraction energy is maximum, the Van der Waals forces overcome the repulsive electrostatic forces and a gel forms. When the quantity of water increases, for example during a subsequent wetting phase, layers of waters are adsorbed onto the particle surfaces, increasing the distance between the particles with a consequent predominance of the long-range repulsive forces and the consequent gel swelling.

Following [8], here the Gouy–Chapman electrical double layer theory has been used to compute the alkali–silica gel expansive pressure starting from the measurement of the net proton surface charge density of the silica gel. Section 2.2 describes the experimental procedure applied in [10] to measure the surface charge density of alkali–silica gel specimens. Then Section 2.3 presents the fundamental equations needed in the computation of the expansive pressure.

2.2. Available experimental results on the surface charge density of ASR gel

For the computation of the alkali–silica gel pressure we have used the experimental data published in [10] on the surface charge density of finely ground particles of alkali–silica gel extracted by the Furnas dam as a function of pH. The concrete dam, located on the Rio Grande river in Minas Gerais (Brazil) and built in 1958–1963, started to show the deterioration symptoms associated with ASR on the quarzite aggregates in 1995. The ASR gel was collected from three different locations in the galleries of the Furnas dam. The ASR gel has been previously characterized by soft X-ray microscopy [24], NMR [25,26] and total scattering methods [27,28]. The NMR results indicated that the silicate network of the ASR gel can be characterized as a layered Q^3-like and clusters of 3-dimensional Q^4 silicates while the pair distribution analysis showed that no distinct structural correlations can be observed beyond about 10 Å. Then the gel was ground by hand to a mean size such that the particles pass the number 300 sieve. Following [29], in [10] the surface charge density of the ASR gel has been measured through potentiometric titrations made over a pH range varying from 10 to 11.5 in electrolyte solutions of 0.7 M NaCl. Actually, the pH of the concrete pore solution reaches values of about 13, value that cannot be easily reached in laboratory tests because of the dissociation of dissolved silica species, as discussed in [29]. The values for the surface charge density experimentally obtained and reported in [10] are shown in Fig. 2 and account for ASR gel dissolution which has been measured gravimetrically at different pH values. The solubility was not affected by pH in the range tested. The values of surface charge for pH = 13.5 has been obtained by extrapolation.

2.3. Gouy–Chapman model and computation of the swelling pressure

We consider two flat adjacent particles in a quiescent electrolyte solution, Fig. 3a shows a schematic representation of the double

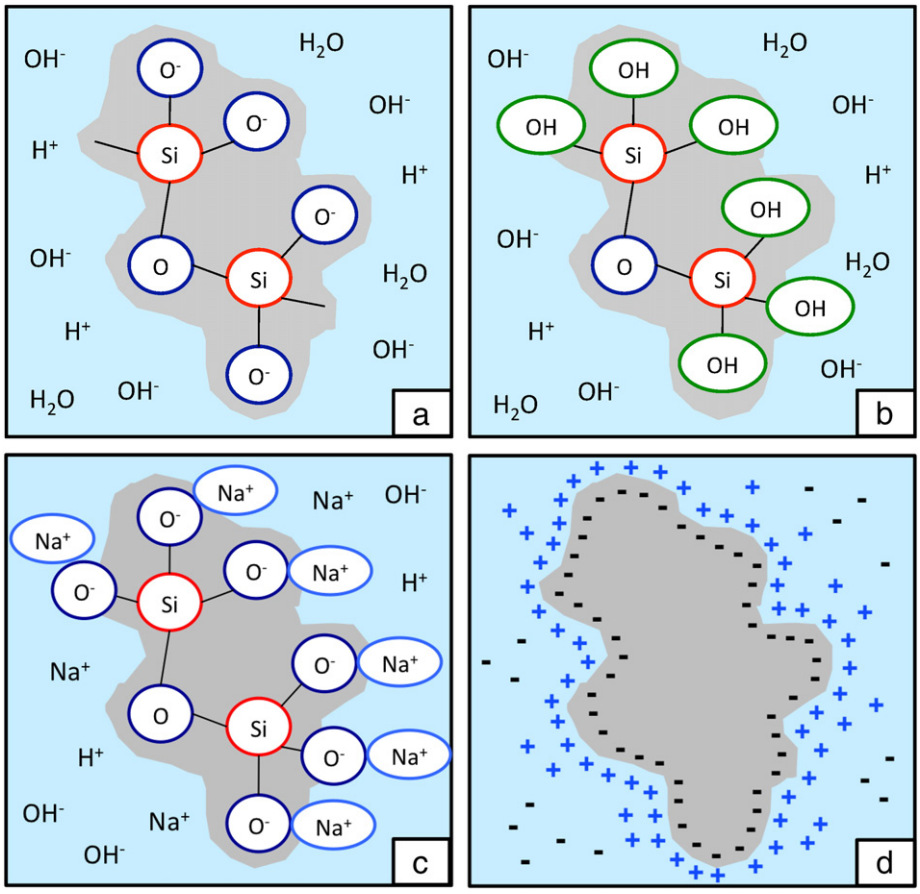

Fig. 1. Schematic representation of the hydration of (a)–(b), a dissolved amorphous silica particle in a high alkaline solution and (c)–(d) the diffuse double-layer around a charged silica particle.

layer of cations in the case of both two interacting negative charged particles and one negative charged particle. The electric field of each charged particle and the cation excess/anion deficit combine to produce a net electric force on its neighbor particle and if the two particles are in close proximity, each one feels the electric potential $\mathcal{V}$ of the other and, as a result, an electric potential $\mathcal{V}_m$ develops midway between them, that is a function of the interparticle distance. The force acting on the planes may be regarded as the sum of the electrostatic force and the osmotic pressure, which arises as a result of the difference between the ionic concentrations of the region inside the particles and the adjacent bulk solution, the charged particle surfaces acting as the membrane separating the regions of high and low concentrations [30]. As underlined in [31], when the system is in equilibrium, at any point of the liquid phase the net electric force is simply balanced by a local pressure gradient

$$\nabla p + \lambda \nabla \mathcal{V} = 0 \tag{1}$$

where p is the pressure, λ is the net ion charge and $\mathcal{V}$ is the electric potential at a point in the solution between the particles. The resulting repulsive pressure p between these two particles can be calculated by integrating the charge density over the potential between the limits $\mathcal{V} = 0$, the reference state where one particle does not feel the presence of the other and hence $p = 0$, and $\mathcal{V}$ which is the electric potential that develops between the particles as result of their interaction

$$p = -\int_0^{\mathcal{V}} \lambda d\mathcal{V}. \tag{2}$$

The relation between the density λ of ions of valence Z, appearing in Eqs. (1) and (2), and the electric potential $\mathcal{V}$ at the distance x from the particle is given by the Poisson's equation

$$\lambda(x) = -\varepsilon_0 \mathcal{D} \frac{d^2 \mathcal{V}(x)}{dx^2} \tag{3}$$

where ε_0 is the permittivity of vacuum and $\mathcal{D}$ the dielectric constant. Moreover, starting from the Boltzmann distribution law of classical statistical mechanics – which gives the concentration of the ions in a force field as a function of the bulk electrolyte concentration C_0 and the

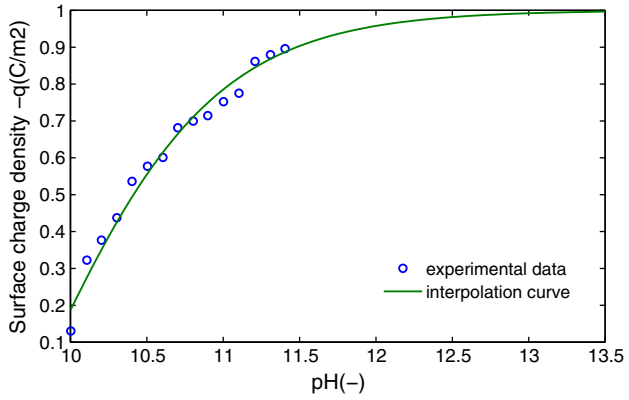

Fig. 2. Measured surface charge for the electrolyte solutions of 0.7 mol/L NaCl: experimental data from [10] and interpolation curve, extrapolated until pH = 13.

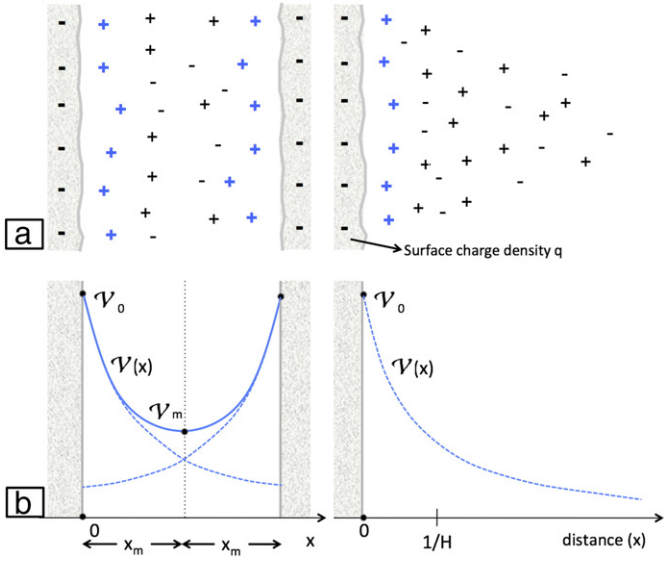

Fig. 3. Schematic representation of (a) the double layer and (b) the electric potential profile $\mathcal{V}(x)$ between two negative charged particle surfaces in comparison with those for a single particle.

electric potential $\mathcal{V}$ – the density λ of ions of valence Z in Eq. (2) can be written in terms of the electric potential $\mathcal{V}$ at the distance x from the particle as

$$\lambda(x) = FZC_0\left\{\exp\left[-Z\frac{\mathcal{V}(x)}{\mathcal{V}_D}\right] - \exp\left[Z\frac{\mathcal{V}(x)}{\mathcal{V}_D}\right]\right\} \tag{4}$$

where $\mathcal{V}_D$ is the potential scaling factor ($\mathcal{V}_D = RT/F = 25.69$ mV at 298 K). In Eq. (4) it is assumed that only one type of cation and one type of anion are present in the diffuse layer, both having the valence Z, F is the Faraday's constant, C_0 is the bulk electrolyte concentration of ions, R is the molar gas constant and T is the absolute temperature. The combination of Eqs. (3) and (4) leads to the Poisson–Boltzmann differential equation

$$\frac{d^2\mathcal{V}(x)}{dx^2} = -\frac{FZC_0}{\varepsilon_0\mathcal{D}}\left\{\exp\left[-Z\frac{\mathcal{V}(x)}{\mathcal{V}_D}\right] - \exp\left[Z\frac{\mathcal{V}(x)}{\mathcal{V}_D}\right]\right\} \tag{5}$$

which gives the electric potential $\mathcal{V}(x)$ at a distance x from the surface of a particle immersed in a solution with bulk electrolyte concentration C_0. More details on the derivation of the Poisson–Boltzmann equation can be found in [19].

Then, the expression of the repulsive pressure can be obtained by Eq. (2), taking into account Eq. (4), and reads

$$p = C_0RT\left[\exp\left(Z\frac{\mathcal{V}}{\mathcal{V}_D}\right) + \exp\left(-Z\frac{\mathcal{V}}{\mathcal{V}_D}\right) - 2\right]. \tag{6}$$

In order to calculate the repulsive pressure from Eq. (6), we need to determine $\mathcal{V}$ from the Poisson–Boltzmann Eq. (5). In the case of two particles (see left scheme in Fig. 3b) the boundary conditions for the Poisson–Boltzmann equation are

$$\mathcal{V} = \mathcal{V}_m \text{ at } x = x_m \text{ and } d\mathcal{V}/dx = 0 \text{ at } x = x_m \tag{7}$$

where x_m is the middle point between two particle surface, and the first integration of the differential Eq. (5) leads to

$$\frac{d\mathcal{V}}{dx} \approx \left[\frac{2RT}{\varepsilon_0\mathcal{D}}C_0(v - v_m)\right]^{\frac{1}{2}} \tag{8}$$

where

$$v = \exp\left(-\frac{Z\mathcal{V}(x)}{\mathcal{V}_D}\right); v_m = \exp\left(-\frac{Z\mathcal{V}_m}{\mathcal{V}_D}\right). \tag{9}$$

Relation (8) is obtained for $\mathcal{V}<0$ and in the particular case of particles with high potential, so that the terms $\exp(Z\mathcal{V}/\mathcal{V}_D)$ and $\exp(Z\mathcal{V}_m/\mathcal{V}_D)$ can be neglected (see [8]).

By combining Eqs. (8) and (9), after some calculations, we obtain

$$\frac{dv}{dx} \approx -Hv(v - v_m)^{\frac{1}{2}}. \tag{10}$$

In the Eq. (10) $1/H$ is referred to as the double layer thickness and its expression is

$$\frac{1}{H} = \sqrt{\frac{\varepsilon_0\mathcal{D}RT}{2F^2Z^2C_0}}. \tag{11}$$

Then the integration of Eq. (10) leads to

$$\sqrt{\frac{v - v_m}{v_m}} = \tan\left(\frac{x_m - x}{2}H\sqrt{v_m}\right). \tag{12}$$

Eq. (12) gives the solution $v(x)$, and hence through definition (9) $\mathcal{V}(x)$, of the Poisson–Boltzmann equation in the case of two interacting flat particles as a function of the midway potential $\mathcal{V}_m$. Fig. 3b shows a schematic representation of this solution (solid line) together with the one, not developed here, relative to single flat particle (dotted lines). The double layer thickness defined in Eq. (11) is the distance of the centroid of the area under the curve $\mathcal{V}(x)$ to the particle surface in this second case. Since when the two double layers of a couple of intercating particles overlap a repulsive force develops, in equilibrium conditions the distance between the particles is $2/H$.

The midway potential $\mathcal{V}_m$, which is usually unknown, can be expressed in terms of the surface charge density at the surface particle q_0, that is the measurable quantity. The surface charge density given by Gouy and Chapman (see [32] and [33]) is

$$q_0 = -\int_0^\infty \lambda(x)dx = \int_0^\infty \varepsilon_0\mathcal{D}\frac{d^2\mathcal{V}(x)}{dx^2}dx = -\varepsilon_0\mathcal{D}\frac{d\mathcal{V}}{dx}. \tag{13}$$

Eq. (13) has been obtained by using the definition of the charge density given by the Poisson's Eq. (3) and considering that $(d\mathcal{V}(x)/dx)_{x=\infty} = 0$. More details can be found in [34].

Finally, the combination of Eqs. (8), (13) and (12), with $x_m = 1/H$, account taken of the definition (9)b, gives the trascendental equation

$$\tan\left[\frac{\sqrt{\exp\left(-\frac{Z\mathcal{V}_m}{\mathcal{V}_D}\right)}}{2}\right] = \frac{-q_0}{\sqrt{2C_0\varepsilon_0\mathcal{D}RT}}\left[\exp\left(-\frac{Z\mathcal{V}_m}{\mathcal{V}_D}\right)\right]^{-\frac{1}{2}}. \tag{14}$$

The electric potential $\mathcal{V}_m$ has been computed using the values of the surface charge reported in Fig. 2 in the Eq. (14), and the ASR gel expansive pressure has been obtained from the relation (6) with $\mathcal{V} = \mathcal{V}_m$. Fig. 4 shows the computed values for the pressure versus pH. These values of the gel pressure can be compared with those obtained with the same theory in [8]. Moreover, they are in the range of those reported in [6] for synthetic ASR gel specimens subject to mechanical tests.

Basic assumptions of the Gouy–Chapman model are that the ions in the diffuse double layer are considered as point charges and there is no interaction between them. Tests on charged platy particles suspended in NaCl solutions show that these assumptions are reasonably accurate for concentrations up to 1 mol L^{-1} (see [35,19]). Moreover in the Gouy–Chapman model the charges are assumed uniformly distributed on the surface of the particle, the particle surface is represented as flat

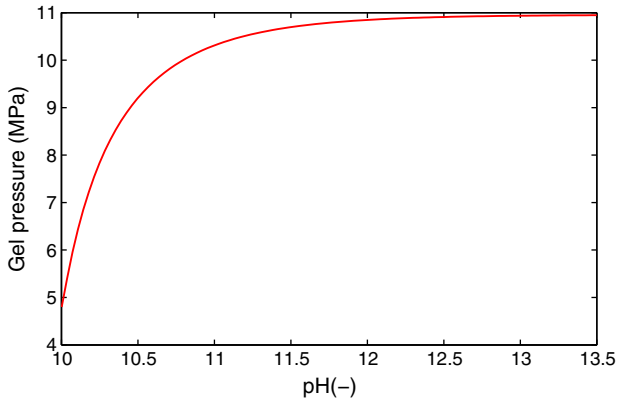

Fig. 4. Values of the alkali–silica gel pressure computed by using the double-layer theory and the surface charge density measured on Furnas dam (Brazil) gel samples.

and infinite and the value of the dielectric constant is considered the same throughout the medium. Many refinements have been proposed over the years in order to remove the limitations of the Gouy–Chapman model (see for example [36–38]) and several surface complexation models have being developed that establish the nature of the interaction between the counterions and the particle surface. Here the Gouy–Chapman model is used in its original form and, despite the simplifications introduced with respect to the real conditions, the results in terms of computed alkali–silica gel expansive pressure are satisfactory.

3. Chemical and mechanical damage model

3.1. Double porosity approach to chemical damage

In the framework of the mechanics of porous materials [39,40], concrete affected by ASR is interpreted as a two-phase heterogeneous material constituted by the homogenized concrete skeleton (s), that includes the cement paste, the aggregates and the non-connected porosity, and the homogenized wet gel (g), which consists of the gel produced by the chemical reaction, the adsorbed water and the gas phases (aqueous vapor and dry air), as shown in Fig. 5a. The two-phase modeling, instead of a three-phase modeling (see e.g. [3] and [41]) in which the gel and the water are considered separately, allows to simplify the formulation without losing the main mechanical aspects. As discussed in [5] this simplification is justified by the lower permeability of concrete with respect to gel than to water, which allows to assume locally drained conditions with respect to the water and locally undrained conditions with respect to the gel. The total volume of the representative volume element V can be expressed as the sum of the volumes occupied by the solid and the wet gel phase, namely $V_s = V - \phi V_0$ and $V_{wg} = \phi V_0$, ϕ being the total concrete Lagrangian porosity and V_0 the initial volume. The volume of the wet gel phase includes the dry gel volume V_g, the liquid water volume V_w and the gas phase volume. The degree of saturation for the water is defined as $S_w = V_w/(V - V_s - V_g)$. For later use we also introduce the definition of the porosity ϕ_w filled by water and gas $\phi_w = (V - V_s - V_g)/V_0$.

In order to model the chemical damage of concrete around the reactive sites, and to take into account the fact that the gel pressure may cause microcracking acting in part in series and in part in parallel with the different portion of the solid matrix, the volume of the homogenized solid skeleton V_s is divided into a part ωV_s which is not affected by chemical damage, with ω material coefficient between 0 and 1, and a part $(1-\omega)V_s$, that represents the portion of concrete which can experience degradation due to ASR, as shown schematically in Fig. 5b. The chemical damage d around the reactive sites is described through an additional porosity ϕ_d which depends exclusively on the reaction extent and grows only in the damageable portion of the reference volume element, see Fig. 5c. According to [42], we assume the following relation between damage and porosity

$$d = 1-(1-\phi_d)^3. \tag{15}$$

Let us consider first the volumetric behavior. The homogenized constitutive equations, relating the total stress $\boldsymbol{\sigma}$ and the total strain $\boldsymbol{\varepsilon}$, can be found by combining the strain partition equations, the stress partition equation and the elastic relations between the volumetric stress and the volumetric strain. The strain partition equations in the whole representative volume element and in its damaged part are given respectively by

$$tr\boldsymbol{\varepsilon} = (1-\phi_0)\omega tr\boldsymbol{\varepsilon}_s + (1-\phi_0)(1-\omega)tr\boldsymbol{\varepsilon}_d + (\phi-\phi_0) \tag{16}$$

$$tr\boldsymbol{\varepsilon}_d = (1-\phi_{d0})tr\boldsymbol{\varepsilon}_s + \phi_d - \phi_{d0} \tag{17}$$

where $tr\boldsymbol{\varepsilon}$ is the total volumetric strain, $tr\boldsymbol{\varepsilon}_s$ is volumetric strain of the undamaged portion and $tr\boldsymbol{\varepsilon}_d$ is the volumetric strain of the damaged portion of the concrete skeleton, $(\phi - \phi_0)$ is the change in concrete porosity, ϕ_0 being the initial concrete porosity, $\phi_d - \phi_{d0}$ is the change in the porosity due to chemical damage, ϕ_{d0} being the initial value, assumed equal to zero. The stress partition equation is given by

$$\boldsymbol{\sigma} = (1-\phi_0)\omega\boldsymbol{\sigma}_s + (1-\phi_0)(1-\omega)\boldsymbol{\sigma}_d - \phi_0 p\mathbf{1} \tag{18}$$

where p is the pressure associated with the change in concrete porosity. Finally the relationships between the mean stress and the volumetric strain for the undamaged (s) and damaged (d) concrete skeleton portions are expressed as

$$\frac{tr\boldsymbol{\sigma}_s}{3} = K_s tr\boldsymbol{\varepsilon}_s, \frac{tr\boldsymbol{\sigma}_d}{3} = (1-d)K_s tr\boldsymbol{\varepsilon}_d \tag{19}$$

with K_s and $(1 - d)K_s$ the bulk moduli of the undamaged and damaged portion of the concrete skeleton respectively.

By combining the Eqs. (16)–(19) the mean total stress can be expressed as

$$\frac{tr\boldsymbol{\sigma}}{3} = \tilde{K}tr\boldsymbol{\varepsilon} - \tilde{K}(\tilde{\phi}-\phi_0) - \phi_0 p \tag{20}$$

where

$$\tilde{K} = \left[\omega + (1-\omega)(1-\phi_d)^3\right]K_s \tag{21}$$

represents a homogenized bulk modulus of the solid skeleton that takes into account the additional porosity created by ASR and

$$\tilde{\phi} = \phi + (1-\omega)(1-\phi_0)\left[1 - \frac{(1-\phi_d)^3}{\omega + (1-\omega)(1-\phi_d)^3}\right]\phi_d \tag{22}$$

is the homogenized total porosity, which includes both the initial concrete porosity ϕ and the porosity ϕ_d due to the chemical damage.

By assuming that the gel pressure p acts both in the concrete porosity ϕ and in the porosity due to micro-cracking ϕ_d at the same time, the following homogenized constitutive equations can be obtained

$$\frac{tr\boldsymbol{\sigma}}{3} = Ktr\boldsymbol{\varepsilon} - bp, \quad \tilde{\phi}-\phi_0 = btr\boldsymbol{\varepsilon} + \frac{p}{N} \tag{23}$$

where K is the macroscopic bulk modulus, $\tilde{\phi}-\phi_0$ is the change in the homogenized total porosity defined in Eq. (22), N and b are the Biot's modulus and coefficient. The Eq. (23) is formally analogous to the constitutive relations originally proposed in [39] and commonly used in poromechanics. In our case the introduction of the additional porosity

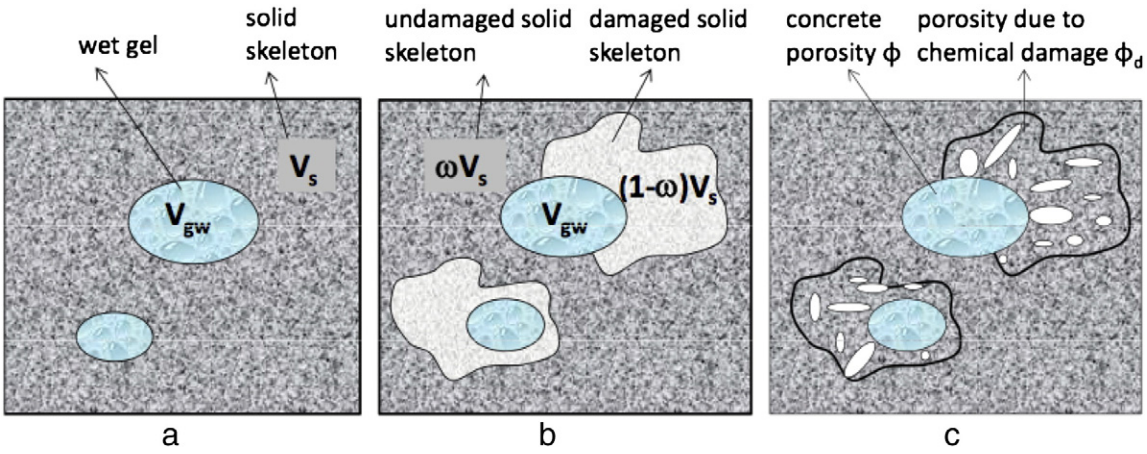

Fig. 5. Schematic representation of the representative volume element of concrete affected by ASR.

ϕ_d leads to a different relationship between the macroscopic coefficients N and b and the microscopic variables with respect to their original expression.

The definition of N and b springs from the combination of Eqs. (20) and (23) (see [40]), that gives

$$b = 1-\frac{K}{\tilde{K}}, \frac{1}{N} = \frac{b-\phi_0}{\tilde{K}}. \tag{24}$$

The modulus $\tilde{K}$ is proportional to the bulk modulus of the concrete skeleton K_s according to the definition (21).

As suggested, e.g. in [43], the gel pressure p can be related to the change in wet gel volume content ζ, defined as the relative change in wet gel mass divided by the gel mass density, instead of the change in porosity. Then, the constitutive Eq. (23) can be rewritten as

$$p = -M(btr\boldsymbol{\varepsilon}-\zeta), \frac{1}{M} = \frac{1}{N} + \frac{\phi_0}{K_g} \tag{25}$$

where M is the Biot's modulus and K_g is the bulk modulus of the fluid (in this case the wet gel) filling the concrete porosity ϕ.

As proposed in [2] and [5] the relative change in wet gel volume content ζ is assumed to be proportional to the reaction extent ξ, a phenomenological variable ($0 \le \xi \le 1$) describing the advancement of the reaction, and reads

$$\zeta = c\xi; c = \frac{K + Mb^2}{Mb}\epsilon^{\infty}_{ASR} \tag{26}$$

The constant c in Eq. (26) is proportional to the free asymptotic volumetric expansion in the isothermal fully saturated case ϵ^{∞}_{ASR} and can be obtained from Eqs. (23) and (25), by imposing the free-stress expansion condition ($\boldsymbol{\sigma} = 0$). In the present model the asymptotic ASR volumetric expansion ϵ^{∞}_{ASR} is considered independent from the states of stress. Indeed, the results obtained in [44] on both stress-free and axially loaded specimens show that directional expansions depend on compressive stresses, which induce the migration of the gel towards the less compressed direction. This hypothesis is well verified for several types of aggregates (see e.g. [45–48,15,17]) while in general it appears as a simplifying assumption (see [49]).

3.2. Simplified micromechanic interpretation

Since the experimental measurements of the homogenized bulk modulus K and the Biot's coefficient b, necessary to solve the system of Eqs. (23) and (25), are usually not available, the relationship between the macroscopic and microscopic variables of the model can be expressed using a simplified micromechanical scheme.

The X-ray images of reacted specimens (e.g. see [7]) suggest the simplified micromechanical scheme sketched in two-dimension in Fig. 6a and consisting of a pore filled with expanding gel surrounded by concrete. The chemical damage due to gel swelling affects only the portion of concrete $(1-\omega)$ disposed radially, while the remaining part of the concrete skeleton ω is undamaged. The mechanical behavior of a such representative volume element can be described by the scheme in Fig. 6b: during its swelling, the gel exerts a pressure on a portion $(1-\omega)$ of the concrete skeleton, working in parallel with the gel, while the rest of the concrete skeleton follows the gel expansion, working in series, without being damaged.

Starting from the equilibrium equations for the system in Fig. 6, the following relations are obtained

$$\frac{tr\boldsymbol{\sigma}}{3} = [(1-\omega)(1-d)K_s]tr\boldsymbol{\varepsilon} - p_{sw} \tag{27}$$

$$p_{sw} = -\frac{\omega K_s K_g}{\omega K_s + K_g}(tr\boldsymbol{\varepsilon} - \bar{c}\xi) \tag{28}$$

where $\bar{c}\xi$ is the expansion of the chemical cell in Fig. 6 and p_{sw} can be interpreted as the swelling pressure (as in [2]).

Comparing Eqs. (27) and (28) with Eqs. (23) and (25) one can obtain a relationship between the macroscopic quantities K and Mb^2 and the microscopic bulk moduli K_s and K_g

$$K = K(d) = (1-\omega)(1-d)K_s, Mb^2 = \frac{\omega K_s K_g}{\omega K_s + K_g}. \tag{29}$$

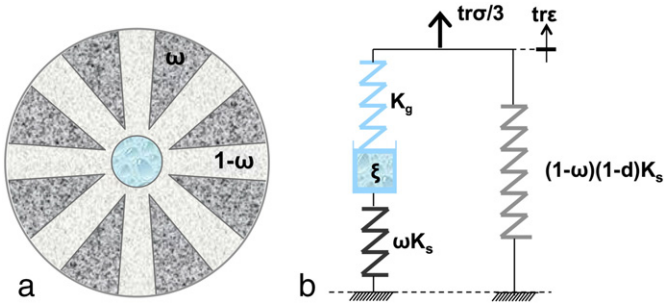

Fig. 6. Schematic representation of the (a) representative volume element and (b) of the volumetric behavior of the proposed model for concrete damage due to ASR.

By using the Eqs. (29), (21) and (15) into Eq. (24), the Biot's coefficient b can be written as functions of the chemical damage d

$$b = \frac{\omega}{\omega + (1-\omega)(1-d)}. \tag{30}$$

Note that while the volumetric modulus term Mb^2 is independent from d (see Eq. (29)) the Biot's parameters M and b separately depend on d. The Eqs. (29)–(30) show that the introduction of the additional porosity ϕ_d brings to a different relationship between these macroscopic coefficients and the microscopic variables with respect to their original expression of the Biot's model. If the chemical damage d reaches its limit value 1, $b = 1$ and Eq. (23) assumes the form introduced by Terzaghi. When $d = 0$, that is the initial situation without damage, $b_0 = \omega$, and for $\omega = 1 - (1 - \phi_0)^3$, the expression $b = 1 - (1 - \phi_0)^3$ proposed in [43] is recovered and the present model reduces to the two-phase chemo-elastic model originally proposed in [2].

By combining the Eqs. (27)–(28) with the relation (29), the relation $\bar{c} = c/b$, between the expansion coefficient $\bar{c}$ appearing in Eq. (28) and the expansion coefficient c defined in Eq. (26), can be found and the swelling pressure p_{sw} can be related to the gel pressure p by the relation $p_{sw} = bp$.

3.3. Three dimensional constitutive model with chemical and mechanical damage variables

The double porosity two-phase model discussed above defines the volumetric behavior of concrete subject to ASR, considering only the chemical damage. For the deviatoric behavior, we assume for the shear modulus the same dependence on the chemical damage obtained for the bulk modulus in Eq. (29).

$$G = G(d) = (1-\omega)(1-d)G_s. \tag{31}$$

This assumption, leading to a constant Poisson's ratio, is quite common in isotropic damage models (see [50]) and is motivated by the lack of precise experimental data on the effect of the ASR on the Poisson's ratio of the concrete. To model the concrete skeleton degradation due to external loads, we also introduce the internal isotropic mechanical damage variable D, depending on the two scalar variables D_t and D_c, respectively referred to prevailing tension and compression conditions $D = 1 - (1 - D_t)(1 - D_c)$. The use of two different damage variables for tension and compression in the context of ASR modeling was previously adopted in [3] and [4]. The state equations, relating the static variables (total Cauchy stress $\boldsymbol{\sigma}$, chemical potential μ_g, chemical energy release rate y, mechanical energy release Y and entropy $\mathfrak{s}$) to the conjugate kinematic variables (strain of the skeleton $\boldsymbol{\varepsilon}$, variation of wet gel phase content ζ, chemical damage d, mechanical damage D and temperature variation $\theta = T - T_0$, T_0 being the local reference temperature), are derived from the free energy potential Ψ.

The following expression for the free energy is proposed:

$$\begin{aligned}\Psi = \Psi(\boldsymbol{\varepsilon}, \zeta, d, D, \theta) = \\ \frac{1}{2}(1-D)\left\{2G(d)\mathbf{e}:\mathbf{e} + K(d)tr^2\boldsymbol{\varepsilon} + Mb^2\left(tr\boldsymbol{\varepsilon} - \frac{\zeta}{b(d)}\right)^2\right\} + \\ \frac{1}{2}(1-D)\left\{-\frac{\mathcal{C}}{T_0}\theta^2 - 2K(d)tr\boldsymbol{\varepsilon}\alpha\theta - 2Mb^2\left(\frac{tr\boldsymbol{\varepsilon}}{b(d)} - \frac{\zeta}{b(d)^2}\right)\alpha_g\theta\right\} \quad + \rho_g\psi_g\zeta.\end{aligned} \tag{32}$$

In the above equation $\mathbf{e}$ is the deviatoric strain tensor, α and α_g, are respectively the volumetric coefficients of thermal expansion for the concrete skeleton and the wet gel, $\mathcal{C}$ is the volumetric heat capacity. The elastic moduli $K(d)$ and $G(d)$ and the Biot's parameters $M(d)$ and $b(d)$, all depending on the chemical damage d, were defined in Eqs. (29), (31) and (30) respectively.

The state equations are obtained by partial derivation and read

$$\boldsymbol{\sigma} = \frac{\partial\Psi}{\partial\boldsymbol{\varepsilon}}, \rho_g\mu_g = \frac{\partial\Psi}{\partial\zeta}, Y = -\frac{\partial\Psi}{\partial D}, y = -\frac{\partial\Psi}{\partial d}, \mathfrak{s} = -\frac{\partial\Psi}{\partial\theta}. \tag{33}$$

The chemical potential μ_g can be expressed in terms of the gel pressure p as

$$\mu_g = \frac{p}{\rho_g} + \psi_g \tag{34}$$

and from Eqs. (32) and (33) one obtains the following expression of the gel pressure

$$p = -(1-D)M(d)\left[b(d)tr\boldsymbol{\varepsilon} - \zeta - \alpha_g\theta\right]. \tag{35}$$

Consequently, the Cauchy stress $\boldsymbol{\sigma}$ defined in Eq. (33) can be written as

$$\boldsymbol{\sigma} = (1-D)[2G(d)\mathbf{e} + K(d)(tr\boldsymbol{\varepsilon} - \alpha\theta)\mathbf{1}] - b(d)p\mathbf{1}. \tag{36}$$

The constitutive model is completed by the evolution equations for the variation of the wet gel volume content ζ, the chemical damage d and the mechanical damage D. According to Eq. (26), the rate of the gel content is proportional to the rate of the reaction extent ξ. The variable ξ is used to describe both the gel formation and the gel swelling, considered as simultaneous, in accordance with the experimental results (see e.g. [51]). Considering a first order reaction kinetics, the following form for the reaction rate is proposed

$$\dot{\xi} = \frac{\left\langle f_{S_w} - \xi \right\rangle^+}{\tilde{t}}, \quad f_{S_w} = \frac{1 + b_1\exp(-b_2)}{1 + b_1\exp(-b_2 S_w)} \tag{37}$$

with b_1 and b_2 material parameters to be calibrated on the basis of experimental data. In the fully saturated case, $S_w = 1$, the kinetic law given in Eq. (37) coincides with the one proposed in [48]. Note that due to the presence of the function $f_{S_w} \leq 1$ in the evolution law, the limit value $\xi = 1$, corresponding to the complete development of the reaction, can be obtained in the fully saturated case only. This limitation of the reaction extent with the saturation degree is also present in the model of [11], where a different kinetic law, depending only on the degree of saturation and not on temperature, was proposed. In Eq. (37) $\tilde{t}$ is the intrinsic time of the reaction, expressed in terms of both the latency time τ_{lat} and the characteristic time τ_{ch} registered for the swelling of reactive specimens and defined in [48]. Several authors focused on the effect of temperature on the intrinsic time (e.g. [2,52,3,4]), in the present work it depends on the local histories of temperature $T(t)$, degree of saturation $S_w(t)$ and reaction extent $\xi(t)$, according to the law proposed in [5], that gives

$$\frac{1}{\tilde{t}} = \frac{\xi/f_{S_w} + \exp(-\tau_{lat}/\tau_{ch})}{\tau_{ch}(1 + \exp(-\tau_{lat}/\tau_{ch}))} \tag{38}$$

with

$$\tau_i(T, S_w) = \left\{\tau_i(\overline{T}, 1) + \frac{\tau_i(\overline{T}, 0) - \tau_i(\overline{T}, 1)}{1 + c_{1i}\exp\left[-\frac{c_{2i}(1-2S_w)}{S_w(1-S_w)}\right]}\right\}\exp\left[U_i\left(\frac{1}{T} - \frac{1}{\overline{T}}\right)\right] \tag{39}$$

with $i = ch, lat$. In the expression (39) the dependence on the temperature, described by the Arrhenius law, is combined with the dependence on the degree of saturation, based on experimental results at the reference temperature $\overline{T} = 38\ ^\circ\mathrm{C}$; U_{lat} and U_{ch} are the activation energies; and the parameters c_{1i} and c_{2i} are calibrated with experimental data. In accordance to the experimental results reported in [48,15] and [44] on highly reactive aggregates we have assumed that the reaction kinetic

is independent from the overall applied stress state. Recent experimental data on concrete with a reactive aggregate composed on chloritic schist obtained in [49], show on the contrary that the presence of an axial compression load affect the reaction kinetic. To model the behavior of that different type of aggregate the Eq. (37) should be modified.

Similarly to what suggested in [53] for the coupling of the mechanical and chemical damage in calcium leached cementitious structures, the chemical damage d is expressed as a function of the reaction extent ξ:

$$d = \frac{1-\exp(-r_1\xi)}{1+\exp(-r_1\xi+r_2)}r_3 \tag{40}$$

where r_1, r_2 and r_3 are material parameters calibrated with the experimental data.

The evolution of the mechanical damage variable D depends on the evolution of the damage in tension D_t and in compression D_c. These latter are governed by loading–unloading conditions defined in terms of the macroscopic stress $\boldsymbol{\sigma}$:

$$f_i \le 0 \dot{D}_i \ge 0 \quad f_i \dot{D}_i = 0, i = t, c. \tag{41}$$

In Eq. (41) f_t and f_c are the damage activation functions in tension and compression, defined as

$$f_i = \frac{1}{2}\mathbf{s}:\mathbf{s} + a_{i0}(tr\boldsymbol{\sigma})^2 + a_{i1}tr\boldsymbol{\sigma}h_i - a_{i2}h_i^2, \quad i = t, c \tag{42}$$

where $\mathbf{s}$ is the deviatoric stress, a_{i0}, a_{i1}, a_{i2} ($i = t, c$) are material parameters governing the shape and dimensions of the elastic domain and h_t and h_c are the hardening–softening functions (see [54] for details).

Since we are introducing a non-standard model, it is necessary to verify the Clausius–Duhem inequality for any damaging process. For an isothermal process this inequality is given by

$$Dissipation = Y\dot{D} + y\dot{d} \ge 0. \tag{43}$$

Starting from the definition of the chemical energy release rate y and the mechanical energy release rate Y (see Eq. (33)), it is possible to demonstrate that in our case the dissipation inequality (43) is satisfied.

3.4. Field equations

In the present model small strains and quasi-static conditions are assumed. As discussed more extensively in [5], the low permeability of concrete with respect to gel allows to neglect its transport, while under partially saturated conditions the migration of the water must be described by an appropriate transport law. Here we adopt the simplified equation of moisture transport in its liquid form proposed in [55], valid for slightly porous materials and obtained by the combination of the Darcy's law for fluid flow in porous media. For a more general formulation one can refer to [56] and [57]. The model takes into account the varying temperature conditions through the heat diffusion equation, based on the combination of the heat conservation law and the Fourier conduction law.

4. Model calibration

The proposed model requires the identification of the following distinct sets of material parameters, namely:

(a) the elastic parameters for concrete matrix and gel G_s, K_s and K_s;
(b) the parameters defining the expansion due to ASR in Eqs. (37)–(39) U_i, $\tau_i(\overline{T},1)$, $\tau_i(\overline{T},0)$, c_{i1} and c_{i2}, with $i = lat, ch$, ϵ^{∞}_{ASR}, b_1 and b_2;
(c) the chemical damage parameters r_1, r_2 and r_3 in Eq. (40) and the parameter ω, which allows to identify the chemically damaged portion of concrete, as shown in Figs. 5 and 6;
(d) the parameters governing the mechanical damage models a_{i0}, a_{i1}, a_{i2}, $i = t, c$ in Eq. (42).

The procedure for the choice of the parameters belonging to the sets (a)–(d) is briefly illustrated in the following.

(a) The elastic parameters for concrete can be computed from the experimental values of Young's modulus and Poisson's ratio. In the following simulations the experimental data reported in [15,16] and [17] are used. The stiffness K_g of the gel filling the concrete porosity is assumed here equal to 6000 MPa. This value can be modified as better quantification becomes available.
(b) For the values of the activation energies U_{lat} and U_{ch} we adopt the values identified in [48] by experiments on reactive specimens at different temperatures. The calibration of the other parameters in Eq. (39), $\tau_i(\overline{T},1)$, $\tau_i(\overline{T},0)$, c_{1i}, c_{2i} and $i = lat, ch$ requires the knowledge of the free expansion curves at different moisture conditions and it is based on the experimental data in [48]. For details on the calibration of these parameters refer to [5], while here we report only the calibrated values in Table 1. Note that these parameters depend not only on the type of reactive aggregates in concrete, but also on their size, as pointed out in [14].
Parameters ϵ^{∞}_{ASR}, b_1 and b_2 in Eqs. (26) and (37) define the maximum free volumetric expansion achievable in different moisture conditions

$$\epsilon_{\max}(S_w) = \epsilon^{\infty}_{ASR}\frac{1+b_1 exp(-b_2)}{1+b_1 exp(-b_2 S_w)}. \tag{44}$$

These parameters have been calibrated by considering the maximum expansion measured in [48] and [15] in isothermal tests on reactive specimens characterized by different degrees of saturation. The values of the parameters thus identified are reported in Table 1. Fig. 7 shows the resulting model curve together with the experimental points reported by several authors.
(c) The amount of the chemically damaged concrete skeleton $(1-\omega)$ and the material parameters r_1, r_2 and r_3 in Eq. (40) can be found using the values of the gel pressure obtained with the double-layer theory in fully saturated conditions – as discussed in Section 2 – and the experimental values of the elastic moduli reduction in function of the deformation due to ASR in a free expansion test. Denoting by $D^{\infty}_{ch} = 1 - (K^{\infty} + Mb^2)/(K_0 + Mb^2)$ the experimental value of the elastic modulus reduction for $\xi \to 1$ and by $\overline{p}$ the value of gel pressure computed by the double-layer theory from the experimental values of the electrical charge density for pH = 13.5

Table 1
Calibrated parameters for the ASR model.

Parameter	Value	Unit	Parameter	Value	Unit
$\tau_{lat}(\overline{T},1)$	70	Days	c_{1lat}	0.03	–
$\tau_{lat}(\overline{T},0)$	145	Days	c_{2lat}	3.1	–
$\tau_{ch}(\overline{T},1)$	20	Days	c_{1ch}	0.004	–
$\tau_{ch}(\overline{T},0)$	80	Days	c_{2ch}	5.0	–
b_1	140,000	–	U_{lat}	9400	K
b_2	18.5	–	U_{ch}	5400	K
ϵ^{∞}_{ASR}	0.009	–			

(see Fig. 4), the combination of Eqs. (26), (29), (30) and (35) for $\xi \to 1$ allows to obtain

$$\frac{(1-D_{ch}^{\infty})\left[(1-\omega)K_s+Mb^2\right]-Mb^2}{\omega} \times\left[\omega+\frac{(1-D_{ch}^{\infty})\left[(1-\omega)K_s+Mb^2\right]-Mb^2}{K_s}\right]\epsilon^{\infty}=\overline{p} \tag{45}$$

from which ω can be computed directly. In this way it is possible to fix the value of ω for a given set of concrete elastic parameters. The microscopic chemical damage variable d evolves in the portion $1-\omega$ of the solid skeleton with the reaction advancement ξ according to Eq. (40). Then, considering that the microscopic chemical damage can be related to the overall elastic moduli reduction by

$$(1-d)=\frac{(1-D_{ch})\left[(1-\omega)K_s+Mb^2\right]-Mb^2}{(1-\omega)K_s} \tag{46}$$

the parameters r_1, r_2 and r_3 are obtained by best fitting from the experimental curve expressing the overall chemical damage D_{ch} as a function of the longitudinal strain, or by Eq. (26), as a function of the reaction extent.

The evolution with the axial expansion of both the microscopic chemical damage d and the overall damage D_{ch} are shown in Fig. 8 together with the experimental data reported in [15] and [16].

The parameters of the set (d) should be computed for each specific concrete and must respect the constraints imposed for the admissibility of the shape of the activation functions as discussed in [54]. The values used in the following examples are reported in Table 3.

Fig. 9a shows the results of the free expansion test reported in [15] at constant temperature and humidity conditions (T = 38 °C, S_w = 0.6) in terms of axial, radial and mean strain versus the duration of the test and the curve obtained by the proposed model with the identified parameters. According to the authors of the experimental tests, the anisotropy of the experimental results is a consequence of the way the concrete has been cast. This effect cannot be reproduced by the present model, therefore the mean strain curve has been used for the calibration. Fig. 9b and c shows the evolution in time of the gel pressure predicted by the model and the corresponding microscopic chemical damage.

Note that in Fig. 9b the gel pressure does not reach its maximum value (here computed equal to 11 MPa in fully saturated case, as explained in Section 2 and shown in Fig. 4) because the test is performed with S_w = 0.6. The chemical damage parameters obtained

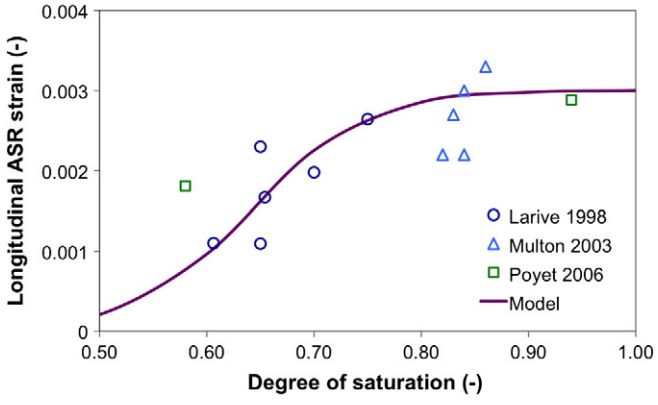

Fig. 7. Variation of the maximum free axial ASR expansion achievable in different moisture conditions: experimental points from [48,15,11] and the model proposed in [5].

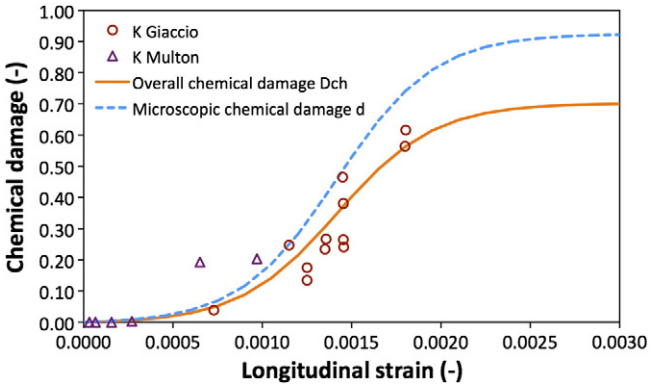

Fig. 8. Evolution of microscopic chemical damage d and of macroscopic damage with longitudinal strain in free expansion tests: experimental points from [16] and [15] and proposed model.

for the concrete used in [15] are reported in Table 2. Fig. 9c shows also the evolution of the Biot's coefficient b with time, as the chemical damage evolves, computed by using Eq. (30).

5. Model validation

5.1. Loaded and confined specimens

The present model for the chemical damage can be validated by simulating several different tests on reactive cylindrical specimens measured during a vast experimental program performed at LCPC (Laboratoire Central des Ponts et Chaussess) and reported in [15]. That experimental program was aimed to study the effect of mechanical stress on the axial and radial expansions due to ASR. In particular axial compressive loads (of 20 MPa), radial confinement obtained by steel rings of 3 mm or 5 mm placed around the specimens and their simultaneous presence were considered. The experimental expansion curves reported in [15] represent the deformations due to the alkali silica reaction only, since they have been obtained by subtracting the creep and the primary shrinkage contribution from the laboratory results. The total deformations measured on reactive specimens can be found in [44].

Figs. 10 and 11 show the evolution of axial and radial strains in loaded, confined and both loaded and confined specimens respectively, always compared with the free expansion tests results used for calibration. The results show that the present model is able to qualitatively reproduce the stress-induced anisotropy due to the application of compressive external loads and confinement. The agreement with the experimental results reported in [15] is quite good, especially if one considers that the model has not been calibrated with the strains obtained in tests on loaded specimens, but only with the experimental value of the gel pressure, the overall Young's modulus reduction and the asymptotic expansion in free expansion tests. Note that the chemical damage evolution as defined in Eq. (40) is independent from the state of stress. Experimental results show that in axially loaded specimens affected by ASR, the microcracking pattern due to ASR is modified with respect to the free expansion case: the microcracks still form, but they tend to align with the compressed direction. When describing the micro-crack pattern at the macro-scale by a single scalar damage value, the information about the crack direction is lost and accordingly we assume that the mean value of the chemical damage is independent from the stress. The poro-mechanical formulation allows nevertheless to obtain the correct anisotropy of strains due to the gel redistribution in the free directions. To consider the change in the micro-crack pattern one should consider an anisotropic damage model as proposed e.g. in [58,3] and [59].

In these tests the compressive stress induced by the external loads or the confinement does not reach the compressive strength of the

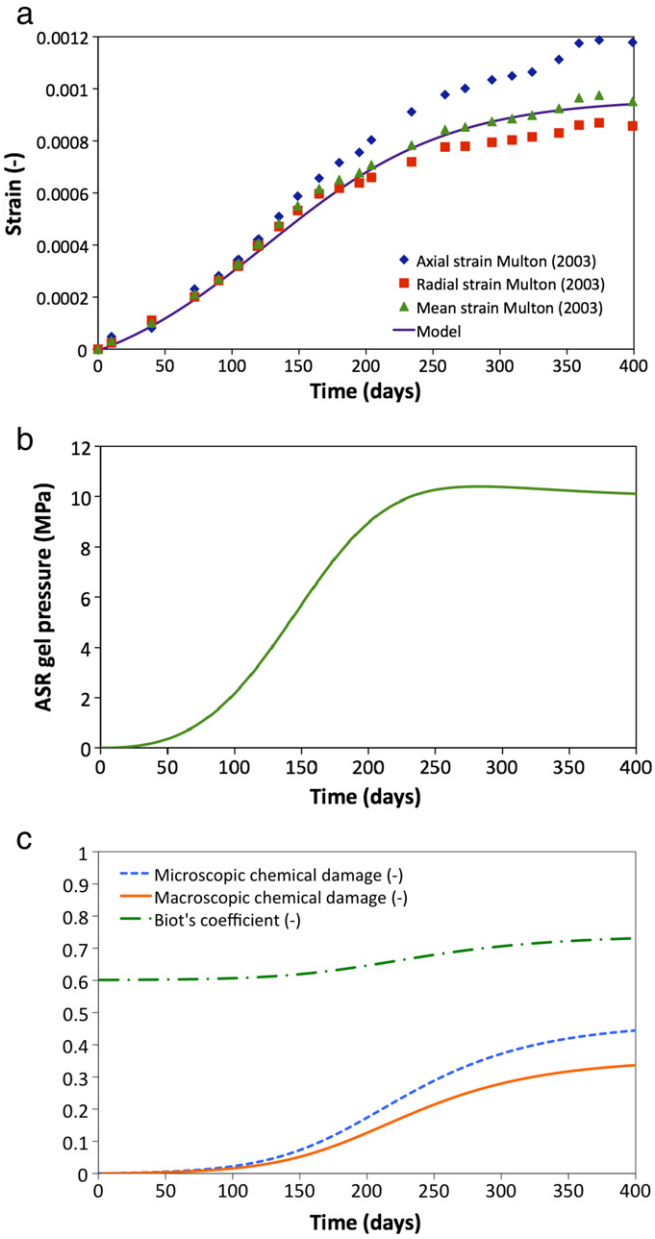

Fig. 9. (a) Evolution of axial, radial and mean strain in the free expansion test ($T = 38$ °C, $S_w = 0.6$): experimental points from [15] and identified model curve. Evolution of the corresponding (b) gel pressure and (c) microscopic and macroscopic chemical damage and Biot's coefficient b predicted by the model.

concrete under examination, thus only the chemical damage activates, while the mechanical damage is not present. The chemical damage parameters are the same used for the calibration (concrete parameters taken from [15]) and reported in Table 2.

Table 2
Parameters governing the chemical damage and used in the numerical examples.

Parameter	Value	Unit	Parameter	Value	Unit
Parameters for Multon [15] and Multon and Toutlemonde [17]					
ω	0.6	–	r_2	5.1	–
r_1	16	–	r_3	0.92	–
Parameters for Giaccio et al. [16]					
ω	0.5	–	r_2	5.2	–
r_1	11	–	r_3	0.92	–

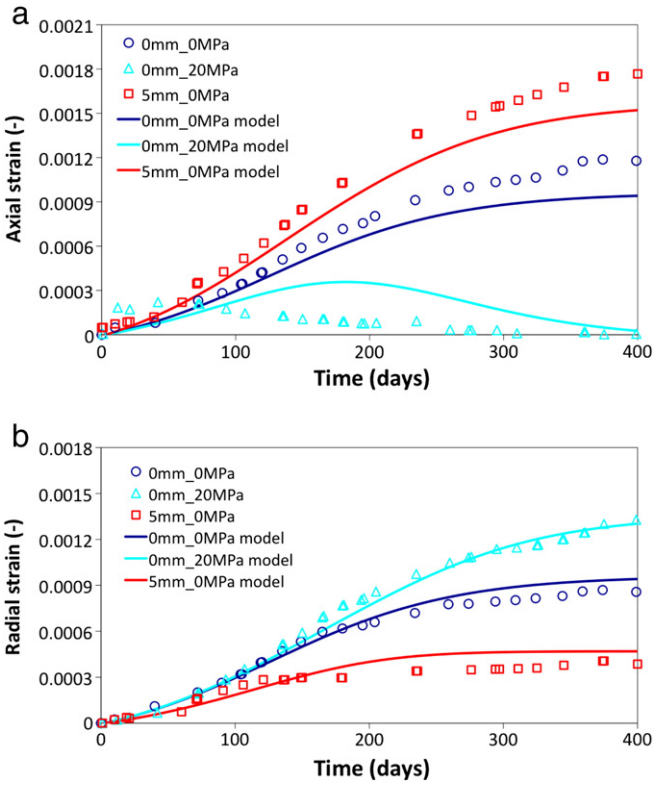

Fig. 10. (a) Axial and (b) radial strains of loaded and constrained (5 mm steel rings) cylindrical specimens (axial stress of 20 MPa) compared with the result of free expansion tests: experimental points from [15] and proposed model.

In order to validate also the coupling between chemical and mechanical damage model, the uniaxial compression tests on cylinders reported in [16] have been simulated. In these tests, the samples of reactive concrete were kept in air in saturated conditions until they reached linear expansions due to ASR in the range of 0.11–0.18%, then mechanical test were performed until failure. The results in [16] were obtained considering various concrete mixtures and show very different overall behaviors depending on the constituents of concrete. In the simulations we have considered the kinetic of the more reactive concrete mixture used in [16] in order to emphasize the effect caused by the activation of ASR. Fig. 12 shows the stress–strain response under uniaxial compression of reactive concrete specimen tested at different times corresponding to ASR expansion of 0.11% and 0.145% together with the model simulation. The model correctly represents the reduction of the initial stiffness due to the evolution of the reaction and observed experimentally through an initial value of the chemical damage (as shown in Fig. 13). The subsequent softening of the response is due to mechanical loads and is obtained in the model as a result of the activation of mechanical damage. Fig. 13 shows the damage evolution corresponding to the two compression tests: the initial value is due to chemical damage, while the subsequent damage, leading to failure, is activated by the compression load. The mechanical damage parameters used for the reactive concrete in the compression test are reported in Table 3. The chemical damage parameters are reported in Table 2.

5.2. Three point bending tests

The model here developed has been implemented in a finite element code through Fortran user's subroutines. The mesh dependence due to the strain localization typical of damageable materials has been prevented adopting a so called "fracture energy regularization" as in [4]. The model has been used to simulate the three-point bending tests on notched specimens reported in [16]. In that experimental

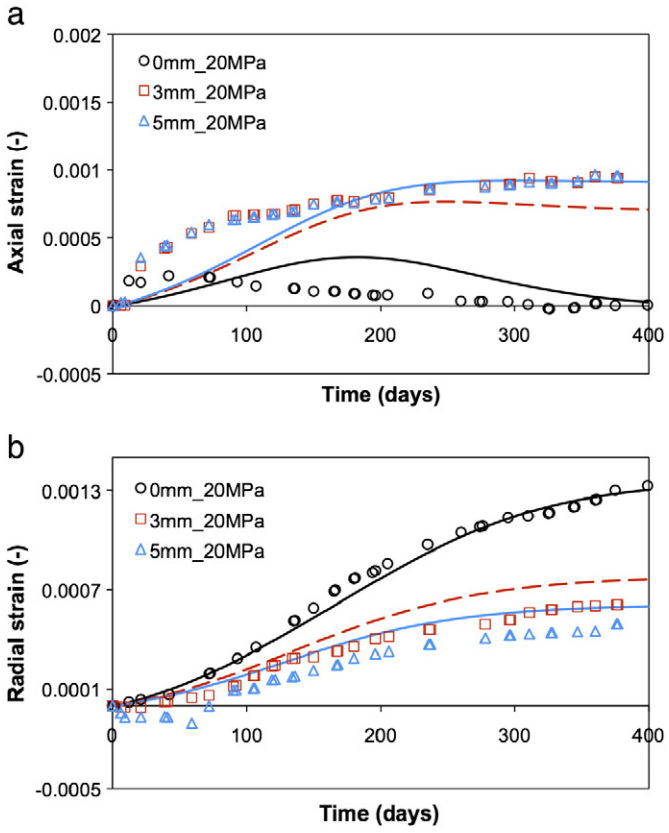

Fig. 11. (a) Axial and (b) radial strains of constrained specimens (3 mm and 5 mm steel rings) under compressive 20 MPa load: experimental points from [15] and proposed model.

program, as for the compression tests, the specimens were cured at 38 °C and bending tests were performed at different times when linear expansion ranging between 0.11% and 0.18% took place. Tests were performed on four different concrete mixtures: the ordinary concrete C1 and the reactive mixtures R2, R3 (the most reactive mixture, considered also in the previous example) and R4. Fig. 14a and b reports the experimental results for the reference ordinary concrete C1 and the reactive mixtures (R2, R3 and R4) reported in [16]. The comparison between the mechanical behavior of different mixtures is made very difficult by the lack of information on mixtures R1, R2 and R3 before the activation of the ASR and by the fact that the mechanical characteristics are influenced by the different composition

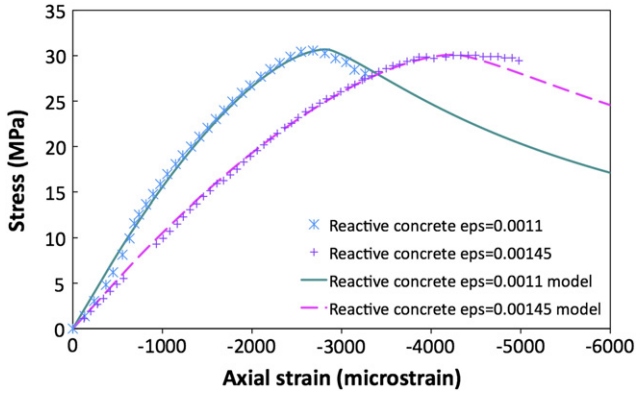

Fig. 12. Stress–strain relation in compression for a reactive concrete at two different reaction extents: experimental points from [16] and proposed model.

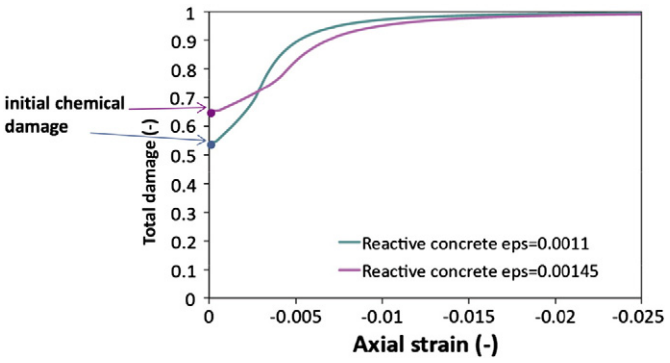

Fig. 13. Damage evolution for a reactive concrete tested in compression at two different reaction extents.

of the concrete even before the evolution of the ASR. In general one can observe that the damage induced by the ASR in the reactive specimen produces an increased non-linearity before the peak and a more gradual softening in the descending branch.

In order to test the capability of the proposed model to describe the effect of the ASR, in this example we referred to a unique set of material parameters, corresponding to the tensile strength of the concrete mixtures C1 and R4, i.e. 3.6 MPa, and we simulated the development of the ASR in this concrete mixture. Fig. 14c reports the load-deflection curves obtained with the model for the specimen in the initial conditions and at 75 and 120 days, when considering the development of the ASR. The model is able to reproduce the experimentally observed increase in ductility, but it is not able to correctly represent the reduction in the tensile strength. This effect could be possibly introduced in the model by modifying the activation of the mechanical damage in order to include the influence of the chemical damage in the hardening functions. As already reported in [58] and as confirmed by the experimental results of [16] reported in Figs. 13 and 14a and b, ASR affects the tensile strength while the compression strength is unaffected. To account for this effect the chemical damage could be introduced in the activation function of the mechanical tensile damage f_t only (see the Eq. (42)). However one should consider that the variability in the experimental results reported in [16] and shown in Fig. 14 makes the modeling of this aspect very difficult. Fig. 14d shows the computed pattern of the mechanical damage in the three-point bending test at 75 days, for an imposed deflection of 1.5 mm. This mechanical damage pattern should be superposed to the chemical one D_{ch} which in this case is uniform, equal to 0.68, to obtain the overall reduction of the elastic properties at each point.

5.3. Reactive unreinforced concrete beams submitted to moisture gradients

Finally the proposed model has been employed to simulate the experimental tests on reactive unreinforced concrete beams reported in [17]. In that experimental program, aimed to investigate the effects of varying humidity conditions on the ASR development, after curing under aluminium sealing, the lower face of the beams was immersed in water, while

Table 3
Mechanical damage coefficients for the reactive concrete.

Parameter	Value	Unit	Parameter	Value	Unit
a_{c0}	0.0025	–	a_{t0}	0.1	–
a_{c1}	3.8	MPa	a_{t1}	6	MPa
a_{c2}	173	MPa^2	a_{t2}	22	MPa^2
γ_c	1.3	–	γ_t	6	–
D_{c0}	0.35	–	D_{t0}	0.5	–
σ_{ec}/σ_{0c}	0.2	–	σ_{et}/σ_{0t}	0.6	–

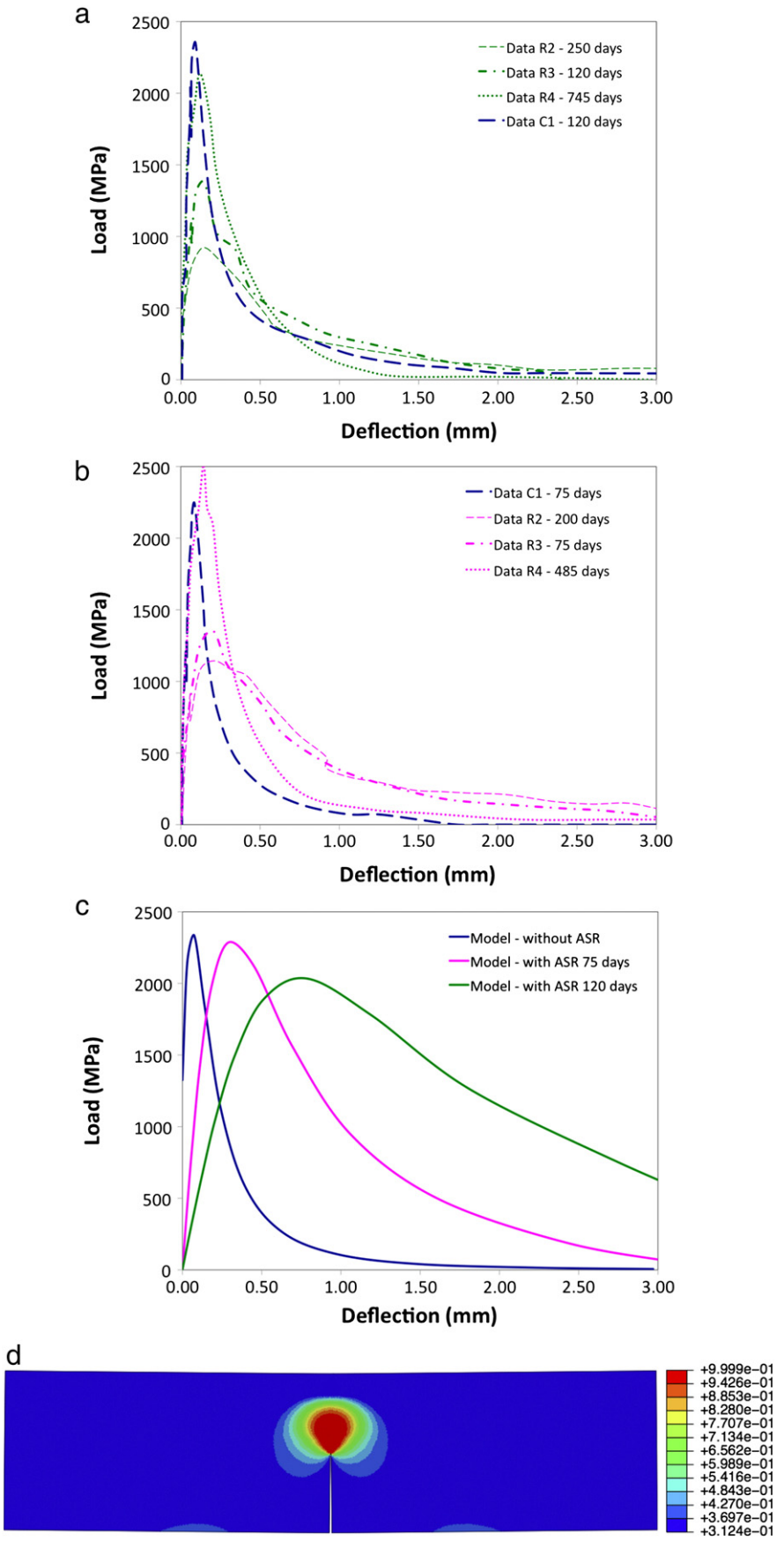

Fig. 14. Flexure test on ordinary and reactive concretes: (a)–(b) experimental results from [16] for ordinary and reactive specimens at different times, (c) curves obtained with the model at different times and (d) computed mechanical damage pattern for the bending test at 75 days.

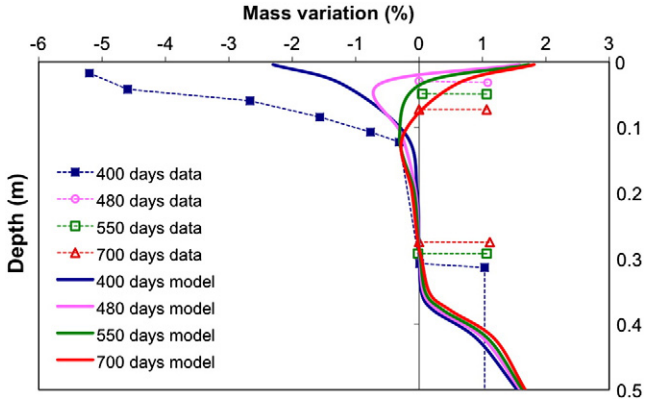

Fig. 15. Mass variation immediately before (400 days) and after (480, 550, 700 days) the re-wetting of the beam: experimental points from Multon and Toutlemonde [17] and model prediction.

the upper face was dried with air at 30% RH for 14 months and then submitted to a delayed water supply for 9 months.

To numerically simulate these tests, first of all a moisture diffusion analysis has been performed to compute the history of the degree of saturation and the corresponding reaction extent history at each point. Fig. 15 compares the experimental results with the model predictions in terms of mass variation along the beam depth at different stages. Even though there is an overall qualitative agreement, point wise there are significant quantitative differences. A careful calibration of the permeability parameters could improve the results but it would require experimental measures of specimen drainage and imbibition for the concrete under examination. Since these experimental data were not available, we have used the permeability parameters reported in the literature for concrete. More details can be found in [5].

Fig. 16 shows the computed patterns of reaction extent and chemical damage after 14 and 23 months respectively. The reaction starts in the lower part of the beam, where humidity is higher, and then, after water supply, develops in the upper part. Then a chemo-mechanical analysis has been performed with the proposed model and Fig. 16c shows the contour plot of damage. In this example only chemical damage activates.

The comparison between experimental results and numerical analysis is shown in Fig. 17 for the plain beam in terms of vertical (a) and transversal (b) strain evolution at different depths of the beam, as indicated on the section of the beam in the same figure. A good qualitative agreement is observed. Fig. 18 shows the corresponding damage evolution in terms of Young's modulus reduction at four depths of the reactive beam. In the upper part (0.08 m depth) a limited damage develops during the first months due to drying, while damage induced by ASR develops after the water supply. The damage evolution is faster in the lower part of the beam, where the degree of saturation is high from the beginning of the experiment and ASR evolves rapidly.

The results in Figs. 16, 17 and 18 can be compared with the results obtained in the same example with other poro-mechanical models (see e.g. [41] and [5]). The present model gives values of damage more realistic than the previous models, with values of the ASR gel pressure in accordance with the experimental data, without sacrificing the results in terms of deformation.

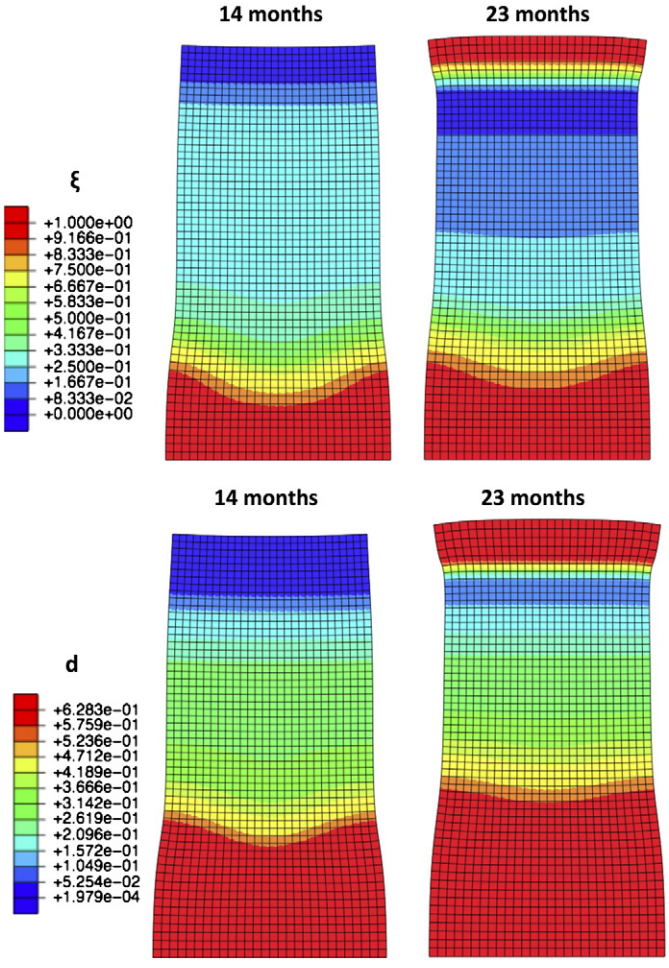

Fig. 16. Patterns of reaction extent and chemical damage after 14 and 23 months.

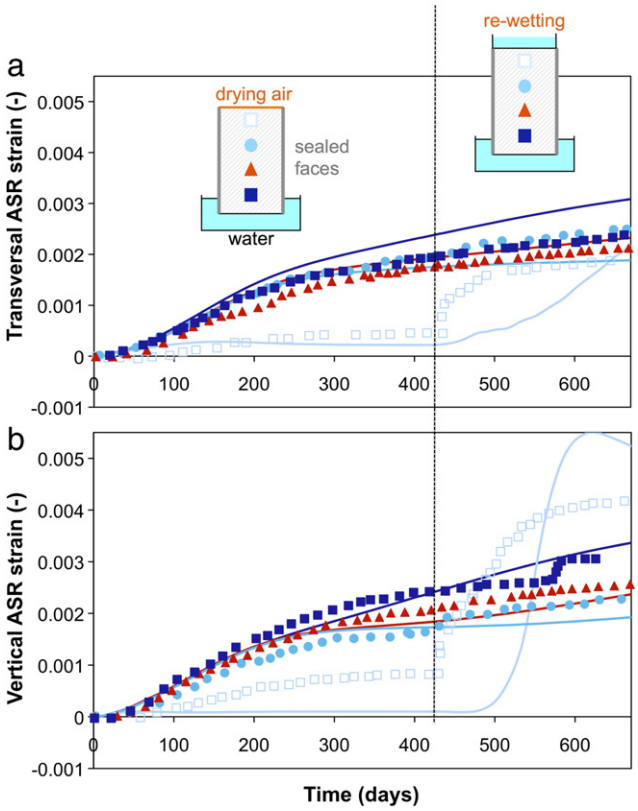

Fig. 17. Transversal (a) and vertical (b) strains of reactive beams measured at four depths (0.08, 0.17, 0.27, 0.37 m from the upper face): experimental points from [17] and model prediction.

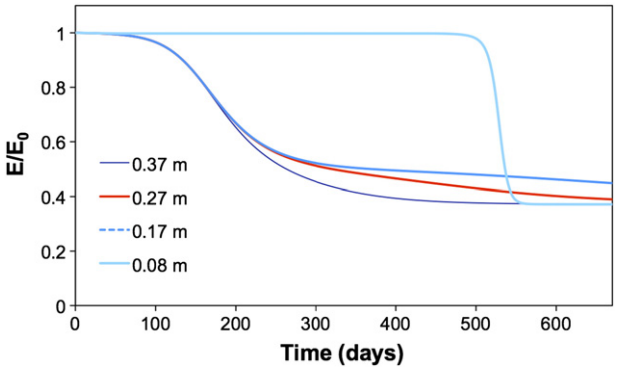

Fig. 18. Young's modulus reduction for the reactive beam computed at four different depths (0.08, 0.17, 0.27, 0.37 m from the upper face): model prediction.

6. Conclusions

In the present work we have developed and validated a new model for the description of degradation in concrete subject to ASR. Two damage mechanisms, the one induced by the chemical reaction and the one induced by the external loads, are considered and described by two independent internal variables. This choice allows for the correct prediction of the overall behavior and the swelling pressure. This latter has been computed in this work using the electrical double layer model as a function of the pH of the pore solution, using experimental data on the surface electrical charge. A microscopic scheme has been proposed to interpret the relationship between the behavior of the material at the micro-scale and the macroscopic behavior. In this paper the model has been applied to simulate various isothermal experimental tests on reacted specimens and beams, also under varying humidity conditions, leading to gradients of the degree of saturation within the structure. One should underline that the chemical damage variable only depends on the reaction extent and its evolution can be easily identified on the basis of free expansion tests. Without any parameters tuning, the model correctly reproduce the effect of loads and confinement on the response of the reacted concrete. Several improvements of the present model appear to be useful for a better prediction of the mechanical behavior of real concrete structures affected by ASR. In particular creep effects and anisotropic mechanical damage should be included in the model and may be considered for further developments.

References

[1] J.W. Pan, Y.T. Feng, J.T. Wang, Q.C. Sun, C.H. Zhang, D.R.J. Owen, Modeling of alkali–silica reaction in concrete: a review, Front. Struct. Civ. Eng. 6 (1) (2012) 1–18.
[2] F.J. Ulm, O. Coussy, L. Kefei, C. Larive, Thermo-chemo-mechanics of ASR expansion in concrete structures, ASCE J. Eng. Mech. 126 (3) (2000) 233–242.
[3] E. Grimal, A. Sellier, Y. Le Pape, E. Bourdarot, Creep, shrinkage, and anisotropic damage in alkali-aggregate reaction swelling mechanism — part I: a constitutive model, ACI Mater. J. 105 (3) (2008) 227–235.
[4] C. Comi, R. Fedele, U. Perego, A chemo–thermo-damage model for the analysis of concrete dams affected by alkali–silica reaction, Mech. Mater. 41 (2009) 210–230.
[5] C. Comi, B. Kirchmayr, R. Pignatelli, Two-phase damage modeling of concrete affected by alkali–silica reaction under variable temperature and humidity conditions, Int. J. Solids Struct. 49 (2012) 3367–3380.
[6] L.J. Struble, S. Diamonds, Swelling properties of synthetic alkali silica gels, J. Am. Ceram. Soc. 64 (11) (1981) 652–655.
[7] M. Kawamura, K. Iwahori, ASR gel composition and expansive pressure in mortars under restraint, Cem. Concr. Compos. 26 (2004) 47–56.
[8] M. Prezzi, P.J.M. Monteiro, G. Sposito, The alkali–silica reation, part 1: use of the double-layer theory to explain the behavior of reaction-product gels, ACI Mater. J. 94 (1) (1997) 10–17.
[9] F.A. Rodrigues, P.J.M. Monteiro, G. Sposito, The alkali–silica reaction the surface charge density of silica and its effect on expansive pressure, Cem. Concr. Res. 29 (1999) 527–530.
[10] F.A. Rodrigues, P.J.M. Monteiro, G. Sposito, A reply to discussion of the paper, 'The alkali–silica reaction the surface charge density of silica and its effect on expansive pressure', Cem. Concr. Res. 41 (2011) 255–262.
[11] S. Poyet, A. Sellier, B. Capra, G. Thevenin-Foray, J.-M. Torrenti, H. Tournier-Cognon, E. Bourdarot, Influence of water on alkali-silica reaction. Experimental study and numerical simulation, J. Mater. Civ. Eng. 18 (4) (2006) 588–596.
[12] H.W. Reinhardt, O. Mielich, A fracture mechanics approach to the crack formation in alkali-sensitive grains, Cem. Concr. Res. 42 (2012) 745–751.
[13] J.M. Ponce, O.R. Batic, Different manifestation of alkali–silica reactionin concrete accordiing to the reaction kinetic of reactive aggregate, Cem. Concr. Res. 36 (2006) 1148–1156.
[14] C.F. Dunant, K.L. Scrivener, Effect of aggregate size on alkali–silica reaction induced expansion, Cem. Concr. Res. 42 (2012) 745–751.
[15] S. Multon, Evaluation experimentale et theorique des effects mechaniques de l'alcali-reaction sur des structures modeles. , PhD thesis LCPC, 2003.
[16] G. Giaccio, R. Zerbino, J.M. Ponce, O.R. Batic, Mechanical behavior of concretes damaged by alkali–silica reaction, Cem. Concr. Res. 38 (2008) 993–1004.
[17] S. Multon, F. Toutlemonde, Effect of moisture conditions and transfer on alkali silica reaction damaged structures, Cem. Concr. Res. 40 (2010) 924–934.
[18] P.C. Carman, Constitution of colloidal silica, Trans. Faraday Soc. 36 (1940) 964–973.
[19] G. Sposito, The surface chemistry of soils, Oxford University Press, New York, 1984.
[20] O. Coussy, P. Dangla, L. Dormieux, E. Lemarchand, A two scale modelling of a swelling clay, J. Phys. IV France 9 (PR9) (2000) 21–31.
[21] L. Dormieux, E. Lemarchand, O. Coussy, Macroscopic and micromechanical approaches to the modelling of the osmotic swelling in clays, Transp. Porous Media 50 (2003) 75–91.
[22] P.C. Hiemenz, Principles of colloid and surface chemistry, Dekker, New York, 1986.
[23] G.H. Bolt, Determination of the charge density of silica sols, J. Phys. Chem. 61 (1957) 1166–1169.
[24] E. Kurtis, P.J.M. Monteiro, J. Brown, W. Meyer-Ilse, Imaging of ASR gel by soft X-ray microscopy, Cem. Concr. Res. 28 (3) (1998) 411–421.
[25] H. Xiaoqiang, L.J. Struble, P.J.M. Monteiro, R.J. Kirkpatrick, Structural investigations of alkali silicate gels, J. Am. Ceram. Soc. 88 (4) (2005) 943–949.
[26] C.E. Tambelli, J.F. Schneider, N.P. Hasparyk, P.J.M. Monteiro, Study of teh structure of alkali–silica reaction gel by high-resolution NMR spectroscopy, J. Non-Cryst. Solids 352 (32–35) (2006) 3429–3436.
[27] C. Benmore, P.J.M. Monteiro, The structure of alkali silicate gel by total scattering methods, Cem. Concr. Res. 40 (6) (2010) 892–897.
[28] C. Meral, C.J. Benmore, P.J.M. Monteiro, The study of disorder and nanocrystallinity in C–S–H, supplementary cementitious materials and geopolymers using pair distribution function analysis, Cem. Concr. Res. 41 (2011) 696–710.
[29] J. Sonnefeld, A. Gobel, W. Vogelsberger, Surface charge density on spherical silica particles in aqueous alkali chloride solutions. Part 1. experimental results, Colloid Polym. Sci. 273 (10) (1995) 926–931.
[30] J. Israelachvili, Intermolecular and surface forces, Academic press, 1992.
[31] H.R. Kruyt, Colloid Science, vol. I, Elsevier publishing, New York, 1952.
[32] G. Gouy, Sur la constitution de la charge eletrque a la surface d'un electrolyte, J. Phys. Theor. Appl. Ser. 49 (1910) 457–468.
[33] L. Chapman, A contribution to the theory of electrocapillarity, Philos. Mag. Ser. 625 (148) (1913) 475–481.
[34] K.M. Kshirendra, G.C. Mishra, M.L. Kansal, Estimation of electric double layer thickness from linearized and nonlinear solutions of Poisson–Boltzmann equation for single type of ions, Appl. Clay Sci. 59–60 (2012) 1–7.
[35] G.M. Torrie, J.P. Valleau, Electrical double layers, 4: limitations of the Gouy–Chapman theory, J. Phys. Chem. 86 (1986) 3251–3257.
[36] O. Stern, Zur theory der electrolytischen doppelschicht, zeitsh, Electrochemistry 30 (1924) 508–516.
[37] D.C. Grahame, The electrical double layer and the theory of electro-capillarity, Chem. Rev. 14 (1947) 441–501.
[38] S.L. Carnie, G.M. Torrie, The statistical mechanics of the electrical double layer, Adv. Chem. Phys. 56 (1984) 141–253.
[39] M.A. Biot, D.G. Willis, The elastic coefficients of the theory of consolidation, J. Appl. Mech. 57 (APM44) (1957) 594–601.
[40] O. Coussy, Poromechanics, John Wiley and Sons, New York, 2004.
[41] C. Comi, R. Pignatelli, A three-phase model for damage induced by ASR in concrete structures, IV International Conference on Computational Methods for Coupled Problems in Science and Engineering, 2011.
[42] K. Kendall, A.J. Howard, J.D. Birchall, The relation between porosity, microstructure and strength, and the approach to cement-based materials, Philos. Trans. R. Soc. Lond. A 310 (1983) 139–153.
[43] F.H. Heukamp, F.J. Ulm, J.T. Germaine, Mechanical properties of calcium-leached cement pastes triaxial stress states and the influence of pore pressures, Cem. Concr. Res. 31 (2001) 767–774.
[44] S. Multon, F. Toutlemonde, Effect of applied stresses on alkali–silica reaction-induced expansions, Cem. Concr. Res. 36 (2006) 912–920.
[45] D.W. Hobbs, Cracking and expansion due to the alkali–silica reaction: its effect on concrete, Struct. Eng. Rev. 2 (1990) 65–70.
[46] N. Clayton, R.J. Currie, R.M. Moss, The effects of alkali–silica reaction on the strength of prestressed concrete beams, Struct. Eng. 68 (15) (1990) 286–292.
[47] G.A. Thompson, R.G. Charlwood, R.R. Steele, D. Curtis, Mactaquac generating station intake and spillway remedial measures, Proceedings of the 18th International Congress on Large Dams, vol. 1, 1994, pp. 347–368.
[48] C. Larive, Apports combines de l'experimentation et de la modelisation la comprehension de l'alcali-reaction et de ses effets mechaniques. PhD thesis LCPC, 1998.
[49] C.F. Dunant, K.L. Scrivener, Effects of uniaxial stress on alkali–silica reaction induced expansion of concrete, Cem. Concr. Res. 42 (2012) 567–576.

[50] J. Lemaitre, J.-L. Chaboche, Mechanics of Solid Materials, Cambridge University Press, 1994.
[51] M. Ben Haha, A. Guidoum, E. Gallucci, K.L. Scrivener, Relation of expansion due to alkali silica reaction to the degree of reaction measured by SEM image analysis, Cem. Concr. Res. 37 (2007) 1206–1214.
[52] V. Saouma, L. Perotti, Constitutive model for alkali-aggregate reactions, ACI Mater. J. 103 (194–202) (2006).
[53] C. Le Bellego, G. Pijaudier-Cabot, B. Gerard, J.F. Dube, L. Molez, Coupled mechanical and chemical damage in calcium leached cementitious structures, J. Eng. Mech. 129 (3) (2003) 333–341.
[54] C. Comi, U. Perego, Fracture energy based bi-dissipative damage model for concrete, Int. J. Solids Struct. 38 (2001) 6427–6454.
[55] V. Baroghel-Bouny, M. Mainguy, T. Lassabatere, O. Coussy, Characterization and identification of equilibrium and transfer moisture properties for ordinary and high performance cementitious materials, Cem. Concr. Res. 29 (1999) 1225–1238.
[56] B.A. Schrefler, F. Pesavento, Multiphase flow in deforming porous material, Comput. Geotech. 31 (2004) 237–250.
[57] F. Pesavento, D. Gawin, M. Wyrzykowski, B.A. Schrefler, L. Simoni, Modeling alkali–silica reaction in non-isothermal, partially saturated cement based materials, Comput. Methods Appl. Mech. Eng. 225–228 (2012) 95–115.
[58] B. Capra, A. Sellier, Orthotropic modelling of alkali-aggregate reaction in concrete structures: numerical simulations, Mech. Meter. 35 (2002) 817–830.
[59] C. Comi, U. Perego, Anisotropic damage model for concrete affected by alkali–silica reaction, Int. J. Damage Mech. 20 (2011) 598–617.